

RoboArmGS: High-Quality Robotic Arm Splatting via Bézier Curve Refinement

Hao Wang^{1*}, Xiaobao Wei^{1*}, Ying Li¹, Qingpo Wuwu¹, Dongli Wu¹, Jiajun Cao¹,
Ming Lu¹, Wenzhao Zheng², Shanghang Zhang^{1†}

¹Peking University; ²University of California, Berkeley

* Equal contribution, † Corresponding author

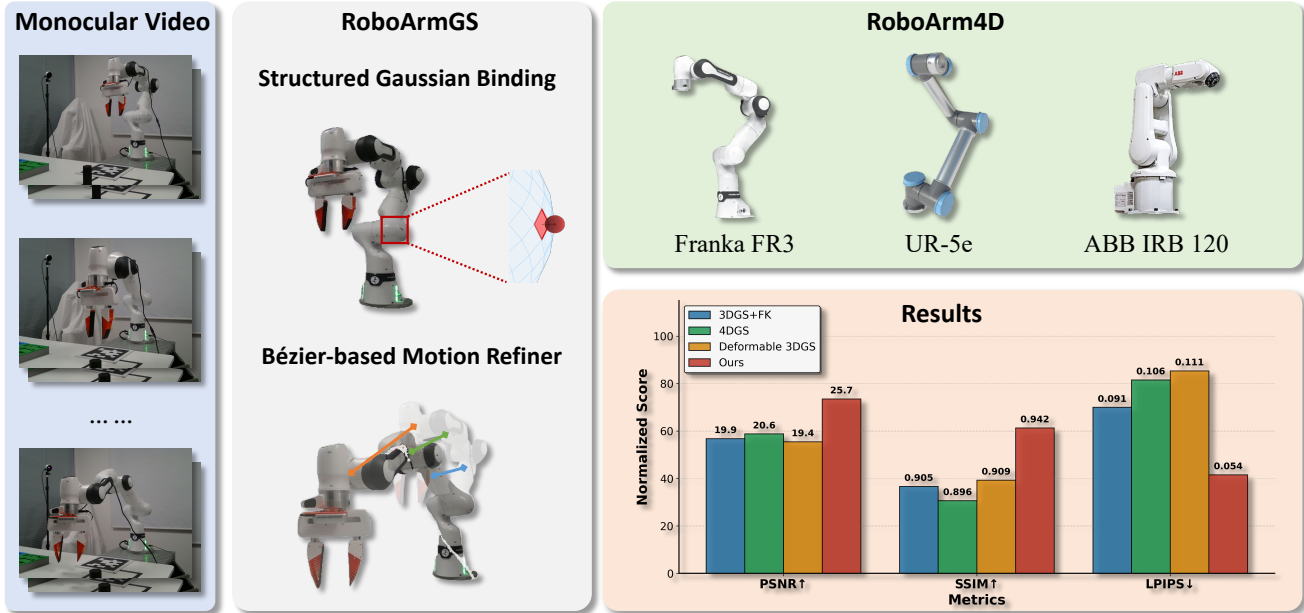


Figure 1. **The illustration of RoboArmGS and RoboArm4D.** We refine URDF-rigged motion with learnable Bézier curves that correct per-joint residuals, bridging the gap between idealized kinematics and noisy real-world dynamics. This enables accurate motion modeling and coherent 3D Gaussian binding across arm parts. We evaluate on RoboArm4D, our carefully collected dataset of widely used robotic arms, achieving state-of-the-art rendering quality.

Abstract

Building high-quality digital assets of robotic arms is crucial yet challenging for the Real2Sim2Real pipeline. Current approaches naively bind static 3D Gaussians according to URDF links, forcing them to follow an URDF-rigged motion passively. However, real-world arm motion is noisy, and the idealized URDF-rigged motion cannot accurately model it, leading to severe rendering artifacts in 3D Gaussians. To address these challenges, we propose RoboArmGS, a novel hybrid representation that refines the URDF-rigged motion with learnable Bézier curves, enabling more accurate real-world motion modeling. To be more specific, we present

a learnable Bézier Curve motion refiner that corrects per-joint residuals to address mismatches between real-world motion and URDF-rigged motion. RoboArmGS enables the learning of more accurate real-world motion while achieving a coherent binding of 3D Gaussians across arm parts. To support future research, we contribute a carefully collected dataset named RoboArm4D, which comprises several widely used robotic arms for evaluating the quality of building high-quality digital assets. We evaluate our approach on RoboArm4D, and RoboArmGS achieves state-of-the-art performance in real-world motion modeling and rendering quality. The code and dataset will be released.

1. Introduction

Robotic arms play a crucial role as the primary executors of tasks in contemporary automation and intelligent systems, making them a significant area of focus in the fields of computer vision and robotics [10, 19, 22, 29]. Reconstructing high-fidelity, interactable digital assets of robotic arms from real-world observations is a foundational step for advancing the Real2Sim2Real pipeline, which is critical for applications in robot control, policy learning, and system monitoring [1, 25, 33]. By generating these digital twins from simple video inputs, we can build simulation environments that faithfully mirror their real-world counterparts. This capability is crucial for bridging the notorious sim-to-real gap, enabling the development and validation of robust control policies in a safe and scalable manner [12, 32]. Consequently, the challenge of automatically generating these dynamic, high-fidelity assets from video remains a key bottleneck in robotics [11, 41]. Overcoming this barrier is crucial for unlocking the vast potential of simulation. It enables large-scale generation of photorealistic, kinematically accurate data, which is essential for training the next generation of general-purpose robotic policies.

Current approaches for building dynamic digital assets of robotic arms typically involve complex, multi-stage pipelines, which hinder their scalability and robustness [7, 15, 20]. This pipeline typically begins with a strictly controlled data capture phase, requiring multi-view images or videos of the scene. Subsequently, the robotic arm must be precisely segmented from the background and other objects, a step that relies on complex segmentation algorithms or, in some cases, even manual annotation of point clouds [20, 44]. This multi-stage pipeline is not only constrained by impractical data capture requirements that limit its use outside the lab but is also highly brittle; slight errors at any stage, particularly in coordinate frame alignment or part segmentation, can cause catastrophic failures in the final model’s fidelity. In contrast, learning directly from a single, casually captured monocular video offers a far more practical and scalable paradigm [14, 30]. While this approach drastically lowers the data collection barrier, it introduces the deeper challenge of accurately modeling the arm’s complex and often non-ideal motion from unstructured observations. This is a problem that rigid, pre-defined kinematic models like Universal Robot Description Format (URDF) struggle to address.

To address these challenges, we propose RoboArmGS (Fig. 1), which introduces a novel hybrid representation that refines the URDF-rigged motion with learnable Bézier curves, enabling more accurate real-world motion modeling. Central to our approach are two key insights: (1) Instead of treating the 3D Gaussians as an unstructured whole, a structured binding mechanism that links them to a geometric prior, such as a mesh, can fundamentally enforce topological consistency. (2) The residual between an idealized kinematic

model like URDF and real-world dynamics can be explicitly modeled and corrected using a flexible, learnable function. Our architecture is built upon these two principles, featuring a novel Gaussian binding strategy and a motion refiner.

Specifically, we first introduce our Structured Gaussian Binding (SGB), which binds each Gaussian to a specific face on the robot’s mesh. To be more precise, each Gaussian is parameterized within the local coordinate frame of its corresponding face, allowing for the learning of its color, opacity, and fine-grained positional offsets. This design ensures that the Gaussians inherit the underlying geometric structure of the robot, while also maintaining the flexibility to capture intricate, real-world appearances. For motion modeling, we then introduce our Bézier-based Motion Refiner (BMR). This module implements a hybrid approach where the URDF-rigged motion provides an idealized motion for the attached Gaussians. On top of this, the BMR learns a continuous-time residual transformation for each joint to precisely compensate for the residuals between the idealized motion and real-world motion. By integrating these two components, RoboArmGS allows for the generation of a statically consistent model while also accurately driving its dynamic motion. This approach significantly reduces rendering artifacts and results in a digital asset with high fidelity in both appearance and motion.

To validate our approach and to provide a standardized benchmark for future research in this area, we further contribute a new, carefully collected dataset, dubbed RoboArm4D. This dataset features several widely used robotic arms and is designed to comprehensively evaluate the quality of high-fidelity digital asset creation.

- We propose RoboArmGS, a novel hybrid representation that uniquely combines Structured Gaussian Binding (SGB) for geometric consistency with a Bézier-based Motion Refiner (BMR) to accurately model real-world motions and mitigate rendering artifacts.
- We introduce RoboArm4D, a new public benchmark dataset specifically designed for the task of creating high-fidelity digital assets of robotic arms from video.
- We conduct extensive experiments demonstrating that RoboArmGS achieves state-of-the-art performance on the RoboArm4D benchmark in both rendering quality and motion accuracy.

2. Related Work

Dynamic Scene Modeling with Gaussian Splatting. 3D Gaussian Splatting (3DGS) has become a widely adopted representation for high-fidelity scene modeling [36, 37, 39]. To capture non-rigid dynamics, Deformable 3DGS [45] introduces a deformation field to model monocular temporal variations. Zhang et al. [38, 48] organize subsets of Gaussian points into graph structures and train graph neural networks to learn object dynamics under physical in-

teractions. In avatar modeling, GaussianAvatars [3, 26] achieve precise parametric control of highly realistic facial avatars by binding discrete 3D Gaussians to a continuous FLAME mesh, jointly optimizing their parameters. Animatable Gaussians [18] extend this Gaussian–mesh binding to full-body avatars using the SMPL template. In the domain of urban scene reconstruction, S³Gaussian [9] and Street-Gaussians [43] achieve high-quality rendering and scene editing by separating Gaussians of moving cars and static background, while HUGS [49] extends Gaussian splatting to additional modalities such as optical flow for improved dynamic modeling. 4DGF [5] adopts a hybrid neural scene representation, combining 3D gaussians as geometric supports with neural fields. OmniRe [4] constructs a dynamic neural scene graph based on 3DGS, generating multiple Gaussian representations for distinct dynamic participants and models pedestrians with the SMPL model. BézierGS [23] introduces learnable Bézier curves to represent vehicle motion trajectories, enforcing geometric consistency via an inter-group curve loss and reducing dependency on precise annotations. Compared to autonomous reconstruction methods that use Bézier curves for naive car motion representation, we employ a Bézier-curve-based correction module to refine an idealized forward kinematics model, aligning it more closely with real-world dynamics.

Robotic Synthesis using 3D Reconstruction. 3D reconstruction serves as a fundamental component for robotic policy learning and data synthesis [2, 21, 34, 47]. Recent research has increasingly leveraged 3DGS to enhance visual realism and geometry-aware robotic simulation. SplatSim [27] replaces traditional mesh-based rendering with 3DGS within simulators, enabling photorealistic RGB data generation for manipulation policy training. RoboGSim [15] utilizes 3DGS to reconstruct scenes and objects from multi-view videos, creating mesh-based digital twins for simulation in Isaac Sim, facilitating demonstration synthesis and closed-loop evaluation. RE³SIM [7] combines 3DGS for background rendering with mesh-based foreground modeling from multi-view stereo while RoboSplat [44] employs a unified 3D Gaussian representation to model the entire workspace (robotic arm, target objects, and background) from multi-view images. More recently, Real2Render2Real [46] scans object with phones, converts 6-DoF object motion trajectories from human demonstration videos into executable robot actions, and leverages IsaacLab for scalable, photorealistic rendering, eliminating the need for simulation and physical hardware. ManipDreamer3D [16, 17] represents scenes via occupancy from monocular images and synthesizes high-fidelity videos conditioned on optimized 3D trajectories. Robo-GS [20] introduces a Gaussian–Mesh–Pixel binding technique to reconstruct static robotic arms and generate operable URDF assets from monocular videos, albeit with strong reliance on accurate panoramic annotations.

In contrast, we bind Gaussian primitives to robot arm meshes and focus on modeling realistic and precise robotic arm motions without requiring panoramic supervision.

3. Methodology

In this section, we introduce RoboArmGS (Fig. 2), our framework for creating high-quality digital twins of robotic arms. Our approach improves 3D Gaussian Splatting through two main contributions: Structured Gaussian Binding, which facilitates physically plausible articulated motion, and a Bézier-based Motion Refiner, designed to correct motion residuals. We also detail the optimization and regularization strategies employed to train our model.

3.1. Preliminaries

3D Gaussian Splatting. 3D Gaussian Splatting [13] is a real-time radiance field method that represents a scene as a collection of 3D Gaussians. Each Gaussian is parameterized by a position μ , rotation q , anisotropic scaling s , opacity α , and Spherical Harmonics for color. During optimization, a valid positive semi-definite covariance matrix Σ is constructed from the learnable scaling and rotation components. To render an image, these 3D Gaussians are projected onto the 2D image plane, sorted by depth, and then composited to compute the final pixel color C via alpha blending:

$$C = \sum_{i \in N} c_i \alpha'_i \prod_{j=1}^{i-1} (1 - \alpha'_j) \quad (1)$$

where c_i is the color of the i -th Gaussian and α'_i is its projected opacity. This entire process is made differentiable and efficient by a dedicated tile-based rasterizer.

Bézier Curves. A Bézier curve [24] is a parametric curve defined by a set of $n + 1$ control points $\{P_i\}_{i=0}^n$. A point on the curve is computed as a weighted sum of these control points using Bernstein basis polynomials as weights:

$$B(t) = \sum_{i=0}^n B_{i,n}(t) P_i, \quad t \in [0, 1] \quad (2)$$

As t varies from 0 to 1, the curve smoothly interpolates the control points, making it an effective tool for modeling smooth trajectories.

3.2. Structured Gaussian Binding

Unlike existing methods that naively bind static 3D Gaussians to URDF links, our Structured Gaussian Binding (SGB) module explicitly binds Gaussians to the kinematic mesh through physics-driven local parameterization and binding-aware adaptive densification. This mesh-level binding ensures motion consistency and structural coherence, effectively integrating kinematic constraints for high-fidelity motion representation.

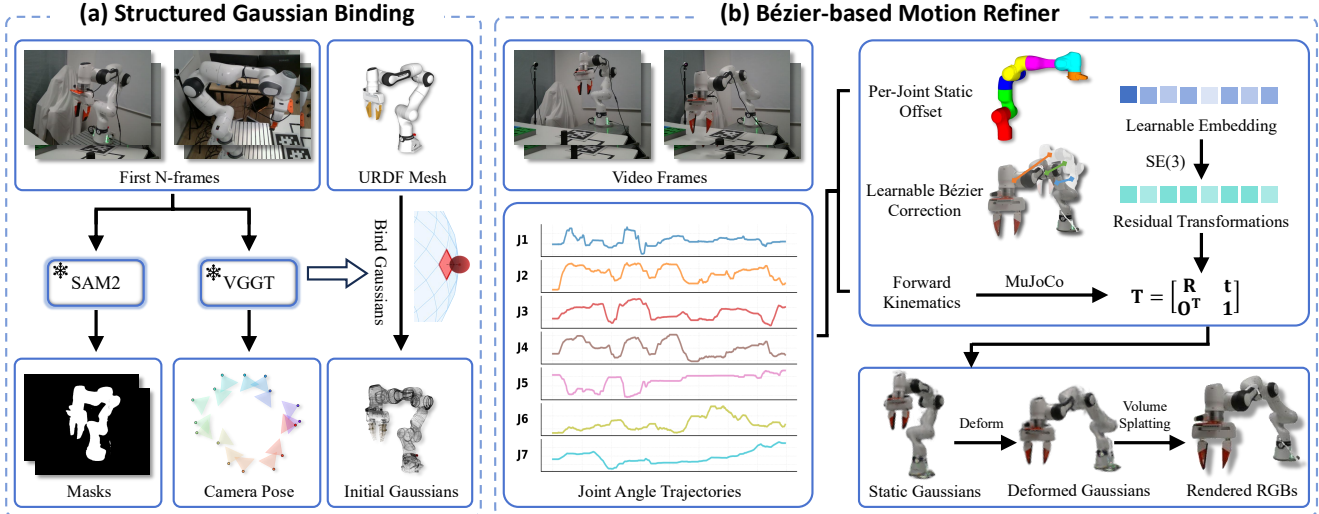


Figure 2. **Overview of RoboArmGS.** Our method consists of two key modules: (a) **Structured Gaussian Binding (SGB)** binds 3D Gaussians according to the URDF links with adaptive densification; (b) **Bézier-based Motion Refinement (BMR)** corrects URDF-rigged motion and real-world motion discrepancies through learnable Bézier curves, enabling accurate novel-pose synthesis. The framework processes multi-view RGB images with known camera poses and robot joint angles, optimizing both modules jointly to achieve photorealistic rendering from novel viewpoints and robot motions.

Physics-driven Local Parameterization. Inspired by recent work [26, 42], we bind each 3D Gaussian to a face on the robot’s kinematic mesh and drive its motion using a physics simulator. Our approach decomposes each Gaussian’s properties into dynamic local-to-world properties and static, learnable properties. The dynamic properties, which include its origin $T_i(t)$, orientation $R_i(t)$, and scaling factor $k_i(t)$, are derived from the mesh vertices after they are transformed by link poses from the MuJoCo engine [31]. The static properties consist of the learnable local attributes (μ_j, r_j, s_j , color, and opacity), which are combined with the dynamic properties for rendering:

$$r'_j(t) = R_i(t)r_j \quad (3)$$

$$\mu'_j(t) = k_i(t) \cdot (R_i(t)\mu_j) + T_i(t) \quad (4)$$

$$s'_j(t) = k_i(t) \cdot s_j \quad (5)$$

This hybrid parameterization ensures physically-plausible motion via the rigid body structure, while simultaneously allowing for the capture of subtle geometric and appearance details through the optimization of local attributes.

Binding-Aware Adaptive Densification. To represent high-frequency details, we adapt the density control from 3DGS [13] with two binding-aware modifications, similar to strategies for rigged avatars [26]. Binding inheritance ensures that new primitives created during densification inherit the parent face index from their progenitor. Additionally, a binding-preservation constraint modifies the standard pruning process to retain at least one Gaussian per face, which

helps to prevent visual holes on occluded surfaces. These adaptations are essential for maintaining the model’s structural integrity during optimization.

3.3. Bézier-based Motion Refiner

While existing methods directly apply Forward Kinematics (FK) transformations without considering the motion process, we introduce a Bézier-based Motion Refiner (BMR) to correct for inevitable discrepancies between idealized FK models and real-world dynamics. It employs a hierarchical decomposition, combining a learnable, time-varying global correction with static, per-joint offsets. This design enforces temporal smoothness globally while allowing for local kinematic flexibility.

Learnable Bézier Correction. The time-varying global correction, $\mathbf{T}_{\text{Bézier}}(t)$, is modeled by a learnable Bézier curve that operates in a 9-dimensional parameter space. We parameterize the residual transformations as 9D vectors $\delta = [\Delta\mathbf{x}, \Delta\mathbf{r}]$, consisting of a 3D translation $\Delta\mathbf{x}$ and a continuous 6D rotation representation $\Delta\mathbf{r}$ [50]. The Bézier curve, defined by $K + 1$ learnable control points $\{\mathbf{p}_k\}_{k=0}^K \subset \mathbb{R}^9$, outputs a 9D residual vector for any time t :

$$\delta_{\text{Bézier}}(t) = \omega \sum_{k=0}^K B_k^K(t) \cdot \mathbf{p}_k \quad (6)$$

where $B_k^K(t)$ are the Bernstein basis polynomials. We use a high-order curve ($K = 19$) to capture complex motion patterns and scale the output by an influence factor ω to

ensure it acts as a subtle refinement. The resulting 9D vector is then converted to a valid SE(3) matrix $\mathbf{T}_{\text{Bézier}}(t)$ via Gram-Schmidt orthogonalization for the rotational part.

Per-Joint Static Correction. The static, per-joint offset, $\mathbf{T}_{\text{embed}}^{(j)}$, is represented by a learnable embedding $\mathbf{e}^{(j)} \in \mathbb{R}^9$ for each moving joint j . These time-invariant embeddings, also parameterized as 9D vectors and initialized to zero, are optimized to correct for local, static errors such as link length discrepancies or joint zero-position offsets. By operating at the joint level, our model directly targets the primary sources of kinematic error within the robot’s articulated structure.

Final Pose Composition. The final refined pose for each joint is computed by sequentially composing the baseline FK pose from MuJoCo with our two learned corrections. The composition order is crucial: the FK pose is first modified by the learnable Bézier correction, and then further refined by the static per-joint offset corresponding to the joint that actuates the joint’s link:

$$\mathbf{T}_{\text{final}}^{(j)}(t) = \mathbf{T}_{\text{FK}}^{(g)}(t) \circ \mathbf{T}_{\text{Bézier}}(t) \circ \mathbf{T}_{\text{embed}}^{(j)} \quad (7)$$

3.4. Optimization and Regularization

The overall optimization of our model is supervised by a combination of a primary rendering loss and several crucial regularization terms designed to ensure geometric stability and temporal coherence.

Rendering Loss. The primary supervision signal is a rendering loss comparing the rendered images with ground truth frames. Following standard practice [13], we use a combination of an L1 photometric loss and a D-SSIM term:

$$\mathcal{L}_{\text{rgb}} = (1 - \lambda)\mathcal{L}_1 + \lambda\mathcal{L}_{\text{D-SSIM}} \quad (\lambda = 0.2) \quad (8)$$

Geometric Regularization. To ensure the optimized Gaussians remain geometrically plausible and well-aligned with their parent faces, we adopt two regularization terms inspired by GaussianAvatars [26]. We penalize the local position offset μ_j and scale s_j if they exceed the thresholds, preventing primitive drifting and visual jittering during animation:

$$\mathcal{L}_{\text{pos}} = \|\max(|\mu_j| - \epsilon_{\text{pos}}, 0)\|_2^2 \quad (9)$$

$$\mathcal{L}_{\text{scale}} = \|\max(|s_j| - \epsilon_{\text{scale}}, 0)\|_2^2 \quad (10)$$

Bézier Velocity Regularization. To enforce that the corrective motions learned by our BMR module are temporally smooth, we regularize the squared L2 norm of the learnable Bézier curve’s instantaneous velocity, $\mathbf{v}(t)$. We approximate this velocity using a numerically stable central difference scheme, and define the loss as:

$$\mathcal{L}_{\text{vel}} = \|\mathbf{v}(t)\|_2^2 \quad (11)$$

This loss penalizes abrupt changes in the learned 9D residual parameters, encouraging a smooth motion trajectory.

Total Objective. Our final training objective is a weighted sum of the aforementioned losses:

$$\mathcal{L}_{\text{total}} = \mathcal{L}_{\text{rgb}} + \lambda_{\text{pos}}\mathcal{L}_{\text{pos}} + \lambda_{\text{scale}}\mathcal{L}_{\text{scale}} + \lambda_{\text{vel}}\mathcal{L}_{\text{vel}} \quad (12)$$

All learnable parameters, including Gaussian attributes, Bézier control points, and per-joint embeddings, are jointly optimized by minimizing this objective.

4. Experiments

4.1. Setup

Settings. We evaluate our method, RoboArmGS, across two challenging settings to assess its reconstruction and motion modeling capabilities. The first setting is Novel-View Synthesis, where the model is trained on multi-view images of a stationary arm and is evaluated on its ability to render photorealistic images from unseen camera viewpoints. The second, more demanding setting is Novel-Pose Synthesis. In this scenario, the model is trained on a video sequence of the arm in motion and is then required to render it from a fixed camera viewpoint, but for a sequence of held-out, unseen joint configurations. Due to space limitations, please refer to the appendix for more experiments.

Datasets. Existing public datasets for robotics typically provide either visual, linguistic, or kinematic data in isolation, making them insufficient for the task of building high-fidelity dynamic digital assets. To address this gap, we introduce RoboArm4D, the first public benchmark specifically designed for creating and evaluating dynamic digital assets of robotic arms. Our dataset features several widely-used industrial arms, such as the Franka Research 3, UR-5e, and ABB IRB 120. For each arm, we offer a complete, synchronized package that includes high-resolution monocular videos, calibrated camera parameters, time-stamped joint trajectories, and the associated URDF file. Additional information regarding the data collection process and the package contents can be found in the supplementary material.

Metrics. To quantitatively evaluate rendering and motion fidelity, we adopt three standard image-based quality metrics: Peak Signal-to-Noise Ratio (PSNR), Structural Similarity Index Measure (SSIM), and Learned Perceptual Image Patch Similarity (LPIPS). These metrics jointly assess both pixel-level accuracy and perceptual quality of rendered views, providing a comprehensive evaluation of real-world motion consistency and rendering fidelity across static and dynamic robotic scenarios.

Novel-View Synthesis				Novel-Pose Synthesis			
Method	PSNR↑	SSIM↑	LPIPS↓	Method	PSNR↑	SSIM↑	LPIPS↓
SuGaR [6]	23.352	0.899	0.106	Deformable 3DGS [45]	19.412	0.909	0.111
Robo-GS [20]	26.061	0.934	0.123	3DGS + FK	19.887	0.905	0.091
2DGS [8]	26.437	0.935	0.118	4DGS [40]	20.582	0.896	0.106
Ours	28.455	0.954	0.051	Ours	25.744	0.942	0.054

Table 1. **Quantitative comparison with state-of-the-art methods.** Our model demonstrates superior performance in both static Novel-View Synthesis (left) and dynamic Novel-Pose Synthesis (right). Green indicates the best and yellow indicates the second-best performance.

Implementation Details. Our model, RoboArmGS, is implemented in PyTorch and trained for 600,000 iterations on a single NVIDIA H100 GPU using the Adam optimizer. For 3D Gaussian attributes, we follow the standard learning rate schedule from 3DGS [13], with position learning rates exponentially decayed to 1% of initial values. The BMR parameters are optimized with a learning rate of 0.0015, weight decay of 0.0001, and influence factor $\omega = 0.1$. Gaussians are initialized by uniform sampling on the kinematic mesh surface, with binding-aware adaptive densification activated every 100 iterations from iteration 500 to 60,000; unstable Gaussian opacities are reset every 3,000 iterations to prune floaters. FK is computed via MuJoCo [31] engine, and regularization hyperparameters are set as $\lambda_{\text{pos}} = 0.01$, $\epsilon_{\text{pos}} = 1.0$, $\lambda_{\text{scale}} = 1.0$, $\epsilon_{\text{scale}} = 0.6$, and $\lambda_{\text{vel}} = 0.001$.

confirms the high fidelity and perceptual realism of our renderings. We attribute this success to our SGB module, which effectively leverages the robot’s kinematic mesh as a powerful geometric prior. By constraining the Gaussians to this structure, our model produces a more coherent 3D representation, establishing a high-quality foundation for dynamic modeling. Fig. 3 provides a qualitative comparison with Robo-GS [20], clearly demonstrating the superior visual quality of our approach.

Novel-Pose Synthesis. We evaluate our dynamic modeling capability on the novel-pose synthesis task, which renders the robot in arbitrary, unseen joint configurations. As shown in Tab. 1, RoboArmGS substantially outperforms all baselines across all metrics. Critically, dynamic scene baselines model [40, 45] temporal evolution using temporal indices rather than kinematic parameters, thus lacking the ability to render from specified joint configurations which is essential for digital twin applications. Even on held-out test frames, their generic deformation models fail to capture articulated motions, producing significant artifacts. The 3DGS + FK baseline, despite correct kinematic positioning, suffers from severe rendering artifacts and structural distortions. Our success stems from the Bézier-based Motion Refiner, which bridges the kinematic modeling gap through temporally smooth global corrections and per-joint offsets, ensuring kinematic accuracy and rendering coherence. Fig. 4 demonstrates our model renders sharp, structurally coherent images precisely aligned with ground truth, validating RoboArmGS as a controllable, motion-accurate digital asset.

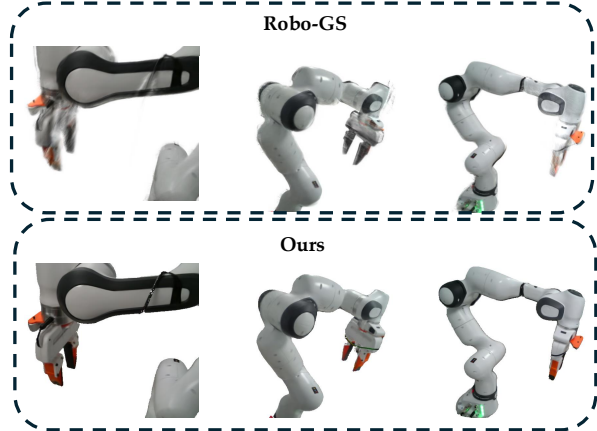


Figure 3. **Qualitative comparison on novel-view synthesis.** Our RoboArmGS achieves significantly sharper and more photorealistic renderings than Robo-GS [20], with better geometric accuracy and texture preservation.

4.2. Main Results

Novel-View Synthesis. We first evaluate the static 3D reconstruction quality on the novel-view synthesis task. As shown in Tab. 1, RoboArmGS demonstrates superior performance, achieving the best results across all metrics, which

4.3. Ablation Study

Module Effectiveness Analysis. We validate the effectiveness of each proposed component through comprehensive ablation studies, presented in Tab. 2. For Novel-View Synthesis, removing the SGB module severely degrades performance. Furthermore, ablating its sub-components confirms their necessity for high-fidelity static reconstruction. For Novel-Pose Synthesis, removing the BMR module demonstrates its critical role in bridging the kinematic modeling gap. As illustrated in Fig. 6, the impact of BMR is

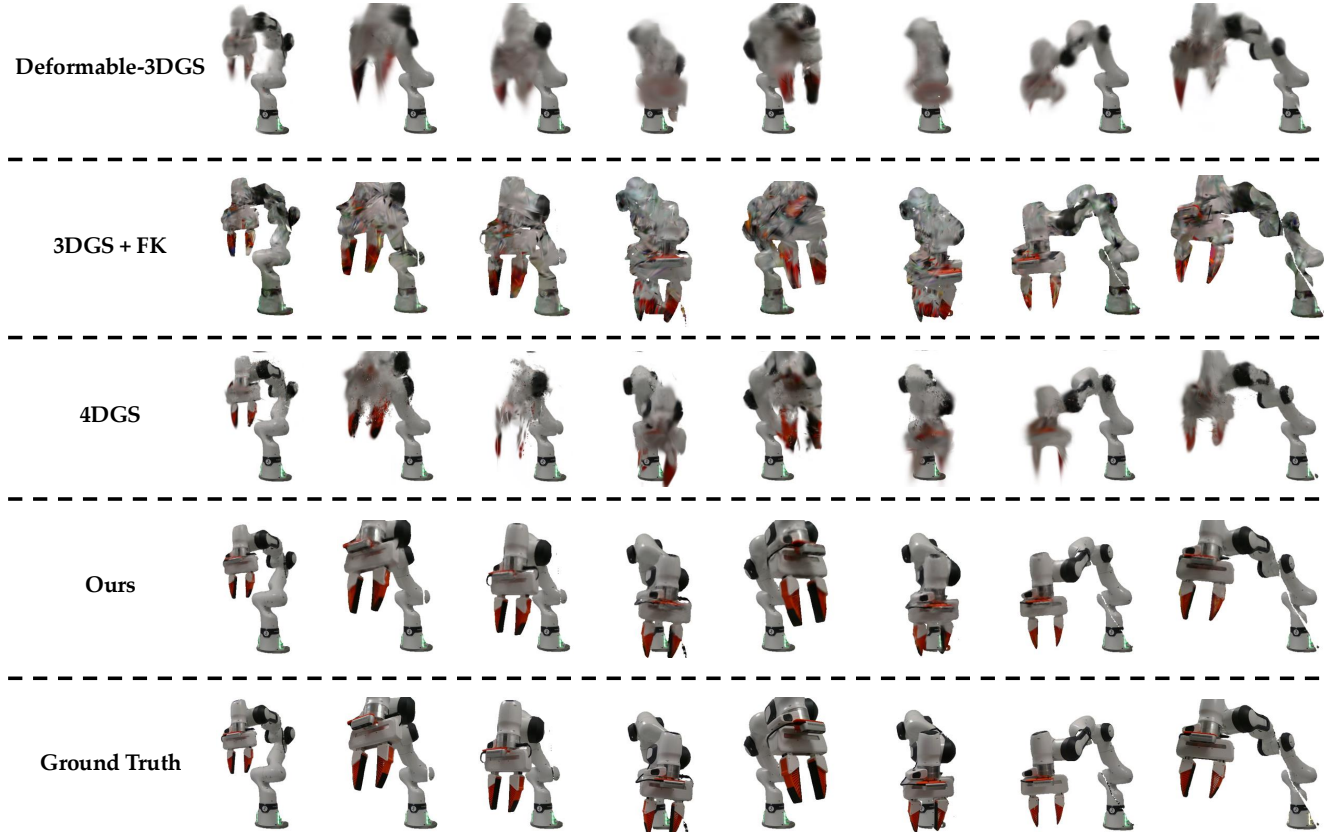


Figure 4. **Qualitative comparison on novel-pose synthesis.** RoboArmGS achieves photorealistic rendering with precise geometric alignment. Baselines fail in different ways: 4DGS and Deformable 3DGS produce blurred, distorted results lacking kinematic control; 3DGS+FK, despite correct Gaussian positioning, generates severe artifacts from inaccurate motion. Our BMR module successfully addresses both motion accuracy and rendering coherence.

Novel-View Synthesis Ablation				Novel-Pose Synthesis Ablation			
Model Variant	PSNR↑	SSIM↑	LPIPS↓	Model Variant	PSNR↑	SSIM↑	LPIPS↓
w/o SGB	20.452	0.809	0.438	w/o BMR	23.484	0.922	0.075
- w/o Adaptive Densification	20.414	0.803	0.451	- w/o Bézier Correction	22.161	0.903	0.089
- w/o Binding	21.621	0.831	0.205	- w/o Per-Joint Offset	24.059	0.929	0.071
Ours (Full Model)	28.455	0.954	0.051	Ours (Full Model)	25.744	0.942	0.054

Table 2. **Quantitative comparison of module effectiveness analysis.** We validate the contributions of our key components on both tasks. The SGB module and its sub-components are crucial for high-quality static reconstruction. The BMR and its sub-components are essential for correcting kinematic errors in novel-pose synthesis. Green indicates the best and yellow indicates the second-best performance.

motion-dependent: the base region (green box), which undergoes minimal motion, shows negligible differences between the full model and the ablated variant, while the gripper region (red box), which experiences large-scale motion, exhibits significant visual artifacts without BMR. Further analysis reveals that both the Learnable Bézier Correction for global dynamic errors and the Per-Joint Static Offset for local static errors are essential and complementary. This study

empirically validates that all proposed components of SGB and BMR are indispensable to the success of RoboArmGS.

Bézier Influence Factor Analysis. We investigate the impact of the influence factor ω , which scales our learnable Bézier correction, with results presented in Tab. 3. Setting $\omega = 0.0$ is equivalent to removing the global correction, which results in the lowest performance and confirms the

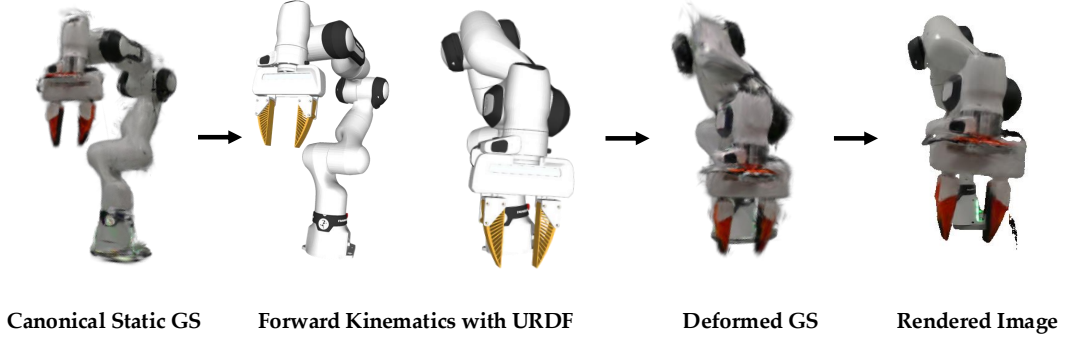


Figure 5. Digital Asset Testing Pipeline. Our trained digital assets enable controllable rendering at test time. Given target joint angles, the URDF-rigged mesh deforms accordingly (left to middle), driving coherent Gaussian transformation via our learned Bézier refinement. The deformed Gaussians render photorealistic images (right) with precise kinematic control.

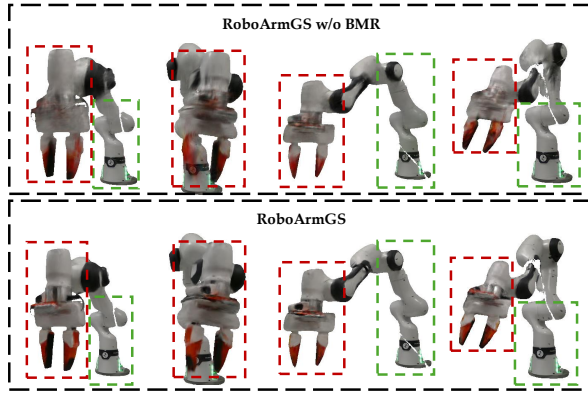


Figure 6. Ablation study visualization. Green box: base region with minimal motion shows similar results for both variants. Red box: gripper region with significant motion reveals rendering artifacts when BMR is removed, demonstrating its importance for high-mobility components.

Influence Factor (ω)	PSNR \uparrow	SSIM \uparrow	LPIPS \downarrow
$\omega = 0.0$	22.161	0.903	0.089
$\omega = 0.01$	24.819	0.940	0.050
$\omega = 0.1$ (Ours)	25.744	0.942	0.054
$\omega = 1.0$	25.509	0.937	0.053

Table 3. Ablation on Influence Factor ω . We analyze the sensitivity of the learnable Bézier correction on the Novel-Pose Synthesis task. A value of $\omega = 0.1$ provides the best balance between effective motion correction and stability. Green indicates the best and yellow indicates the second-best performance.

necessity of this component. As we introduce a small correction factor ($\omega = 0.01$), performance dramatically improves across all metrics. Our chosen value of $\omega = 0.1$ achieves the best PSNR and SSIM scores, striking an optimal balance for overall motion fidelity. However, further increasing ω to

1.0 leads to a slight degradation in performance, suggesting that an overly strong correction can introduce instability or overfitting to the training trajectory. This study validates our selection of $\omega = 0.1$ as an effective and stable choice for motion refinement.

4.4. Digital Assets Visualization

We visualize the interactive testing pipeline of our digital assets in Fig. 5. At test time, users can control the robotic arm in real-time by specifying arbitrary joint angles. The underlying URDF-rigged mesh deforms according to the input kinematics, which are then dynamically refined by our learned Bézier curves to match real-world motion. This refined mesh deformation drives the coherent transformation of all bound 3D Gaussians. These Gaussians are subsequently rendered into photorealistic images from any novel viewpoint, faithfully reflecting the specified pose. By seamlessly integrating a controllable kinematic structure with a high-fidelity neural representation, our digital assets achieve both precise kinematic control and superior rendering quality, enabling flexible and realistic simulation for various downstream applications.

5. Conclusion

We introduce RoboArmGS, a hybrid representation that couples Structured Gaussian Binding with a Bézier-based Motion Refiner to jointly ensure geometric consistency and accurate real-world motion modeling. This design effectively resolves long-standing limitations, including rendering artifacts and URDF-rigged motion mismatch in the robot arm reconstruction. We further release RoboArm4D, the first benchmark dedicated to dynamic robotic arm digital asset reconstruction. Comprehensive experiments show that RoboArmGS achieves state-of-the-art novel-view and novel-pose rendering fidelity.

References

[1] Jad Abou-Chakra, Lingfeng Sun, Krishan Rana, Brandon May, Karl Schmeckpeper, Maria Vittoria Minniti, and Laura Herlant. Real-is-sim: Bridging the sim-to-real gap with a dynamic digital twin for real-world robot policy evaluation. *arXiv e-prints*, pages arXiv–2504, 2025. 2

[2] Ying Chai, Litao Deng, Ruizhi Shao, Jiajun Zhang, Liangjun Xing, Hongwen Zhang, and Yebin Liu. Gaf: Gaussian action field as a dynamic world model for robotic manipulation. *arXiv preprint arXiv:2506.14135*, 2025. 3

[3] Peng Chen, Xiaobao Wei, Qingpo Wuwu, Xinyi Wang, Xingyu Xiao, and Ming Lu. Mixedgaussianavatar: Realistically and geometrically accurate head avatar via mixed 2d-3d gaussians. In *Proceedings of the 33rd ACM International Conference on Multimedia*, pages 945–954, 2025. 3

[4] Ziyu Chen, Jiawei Yang, Jiahui Huang, Riccardo de Lutio, Janick Martinez Esturo, Boris Ivanovic, Or Litany, Zan Gojcic, Sanja Fidler, Marco Pavone, et al. Omnidre: Omni urban scene reconstruction. *arXiv preprint arXiv:2408.16760*, 2024. 3

[5] Tobias Fischer, Jonas Kulhanek, Samuel Rota Bulo, Lorenzo Porzi, Marc Pollefeys, and Peter Kortschieder. Dynamic 3d gaussian fields for urban areas. *arXiv preprint arXiv:2406.03175*, 2024. 3

[6] Antoine Guedon and Vincent Lepetit. Sugar: Surface-aligned gaussian splatting for efficient 3d mesh reconstruction and high-quality mesh rendering. In *Proceedings of the IEEE/CVF Conference on Computer Vision and Pattern Recognition*, pages 5354–5363, 2024. 6

[7] Xiaoshen Han, Minghuan Liu, Yilun Chen, Junqiu Yu, Xiaoyang Lyu, Yang Tian, Bolun Wang, Weinan Zhang, and Jiangmiao Pang. Re3sim: Generating high-fidelity simulation data via 3d-photorealistic real-to-sim for robotic manipulation. *arXiv preprint arXiv:2502.08645*, 2025. 2, 3

[8] Binbin Huang, Zehao Yu, Anpei Chen, Andreas Geiger, and Shenghua Gao. 2d gaussian splatting for geometrically accurate radiance fields. In *ACM SIGGRAPH 2024 conference papers*, pages 1–11, 2024. 6

[9] Nan Huang, Xiaobao Wei, Wenzhao Zheng, Pengju An, Ming Lu, Wei Zhan, Masayoshi Tomizuka, Kurt Keutzer, and Shanghang Zhang. S3gaussian: Self-supervised street gaussians for autonomous driving. *arXiv preprint arXiv:2405.20323*, 2024. 3

[10] Guangqi Jiang, Yifei Sun, Tao Huang, Huanyu Li, Yongyuan Liang, and Huazhe Xu. Robots pre-train robots: Manipulation-centric robotic representation from large-scale robot datasets. *arXiv preprint arXiv:2410.22325*, 2024. 2

[11] Hanxiao Jiang, Hao-Yu Hsu, Kaifeng Zhang, Hsin-Ni Yu, Shenlong Wang, and Yunzhu Li. Phystwin: Physics-informed reconstruction and simulation of deformable objects from videos. *arXiv preprint arXiv:2503.17973*, 2025. 2

[12] Yunfan Jiang, Chen Wang, Ruohan Zhang, Jiajun Wu, and Li Fei-Fei. Transic: Sim-to-real policy transfer by learning from online correction. *arXiv preprint arXiv:2405.10315*, 2024. 2

[13] Bernhard Kerbl, Georgios Kopanas, Thomas Leimkuhler, and George Drettakis. 3d gaussian splatting for real-time radiance field rendering. *ACM Trans. Graph.*, 42(4):139–1, 2023. 3, 4, 5, 6

[14] Qixiu Li, Yu Deng, Yaobo Liang, Lin Luo, Lei Zhou, Chengtang Yao, Lingqi Zeng, Zhiyuan Feng, Huiyi Liang, Sicheng Xu, et al. Scalable vision-language-action model pretraining for robotic manipulation with real-life human activity videos. *arXiv preprint arXiv:2510.21571*, 2025. 2

[15] Xinhai Li, Jialin Li, Ziheng Zhang, Rui Zhang, Fan Jia, Tiancai Wang, Haoqiang Fan, Kuo-Kun Tseng, and Ruiping Wang. Robogsim: A real2sim2real robotic gaussian splatting simulator. *arXiv preprint arXiv:2411.11839*, 2024. 2, 3

[16] Ying Li, Xiaobao Wei, Xiaowei Chi, Yuming Li, Zhongyu Zhao, Hao Wang, Ningning Ma, Ming Lu, and Shanghang Zhang. Manipdreamer: Boosting robotic manipulation world model with action tree and visual guidance. *arXiv preprint arXiv:2504.16464*, 2025. 3

[17] Ying Li, Xiaobao Wei, Xiaowei Chi, Yuming Li, Zhongyu Zhao, Hao Wang, Ningning Ma, Ming Lu, and Shanghang Zhang. Manipdreamer3d: Synthesizing plausible robotic manipulation video with occupancy-aware 3d trajectory. *arXiv preprint arXiv:2509.05314*, 2025. 3

[18] Zhe Li, Zerong Zheng, Lizhen Wang, and Yebin Liu. Animatable gaussians: Learning pose-dependent gaussian maps for high-fidelity human avatar modeling. In *Proceedings of the IEEE/CVF conference on computer vision and pattern recognition*, pages 19711–19722, 2024. 3

[19] Yichao Liang, Kevin Ellis, and Joao Henriques. Rapid motor adaptation for robotic manipulator arms. In *Proceedings of the IEEE/CVF Conference on Computer Vision and Pattern Recognition*, pages 16404–16413, 2024. 2

[20] Haozhe Lou, Yurong Liu, Yike Pan, Yiran Geng, Jianteng Chen, Wenlong Ma, Chenglong Li, Lin Wang, Hengzhen Feng, Lu Shi, et al. Robo-gs: A physics consistent spatial-temporal model for robotic arm with hybrid representation. In *2025 IEEE International Conference on Robotics and Automation (ICRA)*, pages 15379–15386. IEEE, 2025. 2, 3, 6

[21] Guanxing Lu, Shiyi Zhang, Ziwei Wang, Changliu Liu, Jiwen Lu, and Yansong Tang. Manigaussian: Dynamic gaussian splatting for multi-task robotic manipulation. In *European Conference on Computer Vision*, pages 349–366. Springer, 2024. 3

[22] Xiao Ma, Sumit Patidar, Iain Haughton, and Stephen James. Hierarchical diffusion policy for kinematics-aware multi-task robotic manipulation. In *Proceedings of the IEEE/CVF Conference on Computer Vision and Pattern Recognition*, pages 18081–18090, 2024. 2

[23] Zipei Ma, Junzhe Jiang, Yurui Chen, and Li Zhang. B\’eziers: Dynamic urban scene reconstruction with b\’ezier curve gaussian splatting. *arXiv preprint arXiv:2506.22099*, 2025. 3

[24] Michael E Mortenson. *Mathematics for computer graphics applications*. Industrial Press Inc., 1999. 3

[25] Nicholas Pfaff, Evelyn Fu, Jeremy Binagia, Phillip Isola, and Russ Tedrake. Scalable real2sim: Physics-aware asset generation via robotic pick-and-place setups. *arXiv preprint arXiv:2503.00370*, 2025. 2

[26] Shenhan Qian, Tobias Kirschstein, Liam Schoneveld, Davide Davoli, Simon Giebenhain, and Matthias Niessner. Gaussiavatars: Photorealistic head avatars with rigged 3d gaussians. In *Proceedings of the IEEE/CVF Conference on Computer Vision and Pattern Recognition*, pages 20299–20309, 2024. 3, 4, 5

[27] M Nomaan Qureshi, Sparsh Garg, Francisco Yandun, David Held, George Kantor, and Abhishek Silwal. SplatSim: Zero-shot sim2real transfer of rgb manipulation policies using gaussian splatting. In *2025 IEEE International Conference on Robotics and Automation (ICRA)*, pages 6502–6509. IEEE, 2025. 3

[28] Nikhila Ravi, Valentin Gabeur, Yuan-Ting Hu, Ronghang Hu, Chaitanya Ryali, Tengyu Ma, Haitham Khedr, Roman Rädle, Chloe Rolland, Laura Gustafson, et al. Sam 2: Segment anything in images and videos. *arXiv preprint arXiv:2408.00714*, 2024. 1

[29] Baoli Sun, Ning Wang, Xinzhu Ma, Anqi Zou, Yihang Lu, Chuixuan Fan, Zhihui Wang, Kun Lu, and Zhiyong Wang. Robava: A large-scale dataset and baseline towards video based robotic arm action understanding. In *Proceedings of the IEEE/CVF International Conference on Computer Vision*, pages 13985–13994, 2025. 2

[30] Tang Tao, Likui Zhang, Youpeng Wen, Kaidong Zhang, Jia-Wang Bian, Xia Zhou, Tianyi Yan, Kun Zhan, Peng Jia, Hefeng Wu, et al. Robopearls: Editable video simulation for robot manipulation. In *Proceedings of the IEEE/CVF International Conference on Computer Vision*, pages 10118–10129, 2025. 2

[31] Emanuel Todorov, Tom Erez, and Yuval Tassa. Mujoco: A physics engine for model-based control. In *2012 IEEE/RSJ international conference on intelligent robots and systems*, pages 5026–5033. IEEE, 2012. 4, 6

[32] Andrew Wagenmaker, Kevin Huang, Liyiming Ke, Kevin Jamieson, and Abhishek Gupta. Overcoming the sim-to-real gap: Leveraging simulation to learn to explore for real-world rl. *Advances in Neural Information Processing Systems*, 37: 78715–78765, 2024. 2

[33] Boyuan Wang, Xinpan Meng, Xiaofeng Wang, Zheng Zhu, Angen Ye, Yang Wang, Zhiqin Yang, Chaojun Ni, Guan Huang, and Xingang Wang. Embodiedreamer: Advancing real2sim2real transfer for policy training via embodied world modeling. *arXiv preprint arXiv:2507.05198*, 2025. 2

[34] Hao Wang, Xiaobao Wei, Xiaolan Zhang, Jianing Li, Chengyu Bai, Ying Li, Ming Lu, Wenzhao Zheng, and Shanghang Zhang. Embodiedoc++: Boosting embodied 3d occupancy prediction with plane regularization and uncertainty sampler. In *Proceedings of the 33rd ACM International Conference on Multimedia*, pages 925–934, 2025. 3

[35] Jianyuan Wang, Minghao Chen, Nikita Karaev, Andrea Vedaldi, Christian Rupprecht, and David Novotny. Vggt: Visual geometry grounded transformer. In *Proceedings of the Computer Vision and Pattern Recognition Conference*, pages 5294–5306, 2025. 1

[36] Yu Wang, Xiaobao Wei, Ming Lu, and Guoliang Kang. Plgs: Robust panoptic lifting with 3d gaussian splatting. *IEEE Transactions on Image Processing*, 2025. 2

[37] Xiaobao Wei, Peng Chen, Guangyu Li, Ming Lu, Hui Chen, and Feng Tian. Gazegaussian: High-fidelity gaze redirection with 3d gaussian splatting. In *Proceedings of the IEEE/CVF International Conference on Computer Vision*, pages 13293–13303, 2025. 2

[38] Xiaobao Wei, Peng Chen, Ming Lu, Hui Chen, and Feng Tian. Graphavatar: Compact head avatars with gnn-generated 3d gaussians. In *Proceedings of the AAAI Conference on Artificial Intelligence*, pages 8295–8303, 2025. 2

[39] Xiaobao Wei, Qingpo Wuwu, Zhongyu Zhao, Zhuangzhe Wu, Nan Huang, Ming Lu, Ningning Ma, and Shanghang Zhang. Emd: Explicit motion modeling for high-quality street gaussian splatting. In *Proceedings of the IEEE/CVF International Conference on Computer Vision*, pages 28462–28472, 2025. 2

[40] Guanjun Wu, Taoran Yi, Jiemin Fang, Lingxi Xie, Xiaopeng Zhang, Wei Wei, Wenyu Liu, Qi Tian, and Xinggang Wang. 4d gaussian splatting for real-time dynamic scene rendering. In *Proceedings of the IEEE/CVF conference on computer vision and pattern recognition*, pages 20310–20320, 2024. 6

[41] Ziyang Xie, Zhizheng Liu, Zhenghao Peng, Wayne Wu, and Bolei Zhou. Vid2sim: Realistic and interactive simulation from video for urban navigation. In *Proceedings of the Computer Vision and Pattern Recognition Conference*, pages 1581–1591, 2025. 2

[42] Yuelang Xu, Benwang Chen, Zhe Li, Hongwen Zhang, Lizhen Wang, Zerong Zheng, and Yebin Liu. Gaussian head avatar: Ultra high-fidelity head avatar via dynamic gaussians. In *Proceedings of the IEEE/CVF conference on computer vision and pattern recognition*, pages 1931–1941, 2024. 4

[43] Yunzhi Yan, Haotong Lin, Chenxu Zhou, Weijie Wang, Haiyang Sun, Kun Zhan, Xianpeng Lang, Xiaowei Zhou, and Sida Peng. Street gaussians: Modeling dynamic urban scenes with gaussian splatting. In *European Conference on Computer Vision*, pages 156–173. Springer, 2024. 3

[44] Sizhe Yang, Wenyue Yu, Jia Zeng, Jun Lv, Kerui Ren, Cewu Lu, Dahua Lin, and Jiangmiao Pang. Novel demonstration generation with gaussian splatting enables robust one-shot manipulation. *arXiv preprint arXiv:2504.13175*, 2025. 2, 3

[45] Ziyi Yang, Xinyu Gao, Wen Zhou, Shaohui Jiao, Yuqing Zhang, and Xiaogang Jin. Deformable 3d gaussians for high-fidelity monocular dynamic scene reconstruction. In *Proceedings of the IEEE/CVF conference on computer vision and pattern recognition*, pages 20331–20341, 2024. 2, 6

[46] Justin Yu, Letian Fu, Huang Huang, Karim El-Refai, Rares Andrei Ambrus, Richard Cheng, Muhammad Zubair Irshad, and Ken Goldberg. Real2render2real: Scaling robot data without dynamics simulation or robot hardware. *arXiv preprint arXiv:2505.09601*, 2025. 3

[47] Tengbo Yu, Guanxing Lu, Zaijia Yang, Haoyuan Deng, Season Si Chen, Jiwen Lu, Wenbo Ding, Guoqiang Hu, Yansong Tang, and Ziwei Wang. Manigaussian++: General robotic bi-manual manipulation with hierarchical gaussian world model. *arXiv preprint arXiv:2506.19842*, 2025. 3

[48] Mingtong Zhang, Kaifeng Zhang, and Yunzhu Li. Dynamic 3d gaussian tracking for graph-based neural dynamics modeling. *arXiv preprint arXiv:2410.18912*, 2024. 2

- [49] Hongyu Zhou, Jiahao Shao, Lu Xu, Dongfeng Bai, Weichao Qiu, Bingbing Liu, Yue Wang, Andreas Geiger, and Yiyi Liao. Hugs: Holistic urban 3d scene understanding via gaussian splatting. In *Proceedings of the IEEE/CVF Conference on Computer Vision and Pattern Recognition*, pages 21336–21345, 2024. [3](#)
- [50] Yi Zhou, Connelly Barnes, Jingwan Lu, Jimei Yang, and Hao Li. On the continuity of rotation representations in neural networks. In *Proceedings of the IEEE/CVF conference on computer vision and pattern recognition*, pages 5745–5753, 2019. [4](#)

RoboArmGS: High-Quality Robotic Arm Splatting via Bézier Curve Refinement

Supplementary Material

A. Overview

This appendix provides supplementary details regarding the proposed RoboArm4D dataset and presents additional experimental evaluations for RoboArmGS. We first elaborate on the dataset construction in the following section, covering the hardware specifications, data capture protocols, and the processing pipeline used to generate the monocular sequences. Subsequently, we report extended quantitative and qualitative results on the Universal Robots UR5e and ABB IRB 120 sequences. These additional experiments on Novel-View Synthesis and Novel-Pose Synthesis further validate the generalizability and high-fidelity rendering capabilities of our method across diverse robotic morphologies.

B. The RoboArm4D Dataset Details

To facilitate research in high-fidelity robotic arm reconstruction and motion modeling, we introduce the RoboArm4D dataset. This dataset features monocular video sequences of several common robotic arms performing diverse motions. This section provides a detailed overview of our data capture hardware, protocol, and processing pipeline.

B.1. Hardware Setup

Our data collection setup was designed for simplicity and accessibility, requiring minimal specialized equipment. We captured all sequences using a single, handheld Intel RealSense L515 camera, recording RGB video at a resolution of 640x480 and a rate of 30 frames per second to simulate casual capture conditions. The dataset features three widely-used robotic arms: the Franka Research 3 (7-DoF), the Universal Robots UR5e (6-DoF), and the ABB IRB 120 (6-DoF). Each arm was mounted on a workbench within a standard laboratory environment, characterized by diffuse overhead lighting and a relatively static, yet typical, background containing various lab equipment.

B.2. Data Capture Protocol

B.2.1. Camera Pose Calibration

Accurately determining the pose of a static camera is crucial. To achieve this, we first captured a short calibration video (approx. 30 seconds) where the handheld camera was moved extensively around the static robotic arm and its environment. This multi-view sequence was processed using VGGT [35] to generate a sparse 3D reconstruction of the scene and to precisely compute the camera poses for each frame of the calibration video. From this set of calibrated poses, we selected a single, fixed viewpoint for the subsequent motion

capture. This process effectively pre-calibrates the static camera's extrinsic parameters within the scene's coordinate frame.

B.2.2. Motion Trajectory and Recording

With the camera now fixed in its pre-calibrated position, the robotic arm was programmed to execute a pre-defined, smooth trajectory. These trajectories were designed to cover a wide range of joint configurations, including both simple single-joint movements and complex multi-joint coordinated motions. While the arm was in motion, we recorded a continuous video sequence from the static viewpoint. Each motion sequence lasts approximately 30-60 seconds, resulting in 900-1800 frames. Simultaneously, joint angles were recorded directly from the robot's controller API to be synchronized with the video frames during post-processing.

B.2.3. Data Processing Pipeline

The raw video and joint angle data were processed into a format suitable for training our model using the following steps:

- **Video to Frames:** The captured videos were decomposed into individual PNG frames.
- **Camera Pose Estimation:** We used VGGT [35] to estimate the camera intrinsics and the per-frame extrinsic poses (camera-to-world transformation). Poses were optimized over the entire sequence to ensure global consistency.
- **Foreground Segmentation:** To separate the robotic arm from the background, we employed the Segment Anything Model 2 (SAM2) [28]. We provided a few initial keyframe masks, and SAM2 [28] automatically propagated the segmentation to the entire sequence, followed by minor manual refinement where necessary. This resulted in a pixel-perfect foreground mask for each frame.
- **Data Synchronization:** The high-frequency joint angle data were synchronized with the video frames. We used linear interpolation to obtain the precise joint angle configuration corresponding to the capture time of each frame.

B.3. Dataset Splitting Protocol

We adopt a uniform sampling strategy to partition the dataset into training, validation, and test sets with an 8:1:1 ratio. Specifically, we select every 10th frame for the test set and every 10th frame for the validation set, ensuring distinct frames for each subset (non-overlapping). The remaining frames constitute the training set. This interval-based splitting ensures that the evaluation covers the full range of motion and viewpoints present in the recorded sequences.

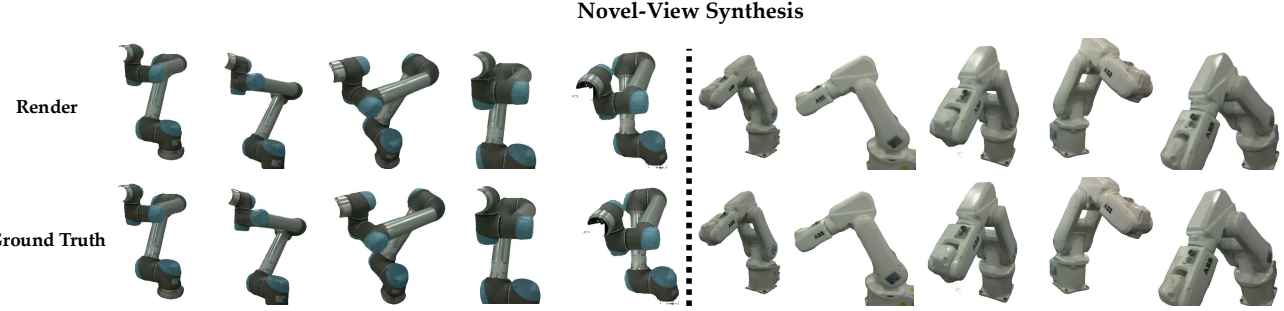


Figure 1. **Qualitative results for Novel-View Synthesis.** RoboArmGS synthesizes photorealistic images from unseen viewpoints for both the Universal Robots UR5e (left) and ABB IRB 120 (right). Our method faithfully reconstructs high-frequency details and preserves the visual fidelity of the robot’s appearance, while maintaining sharp geometric boundaries against the background.

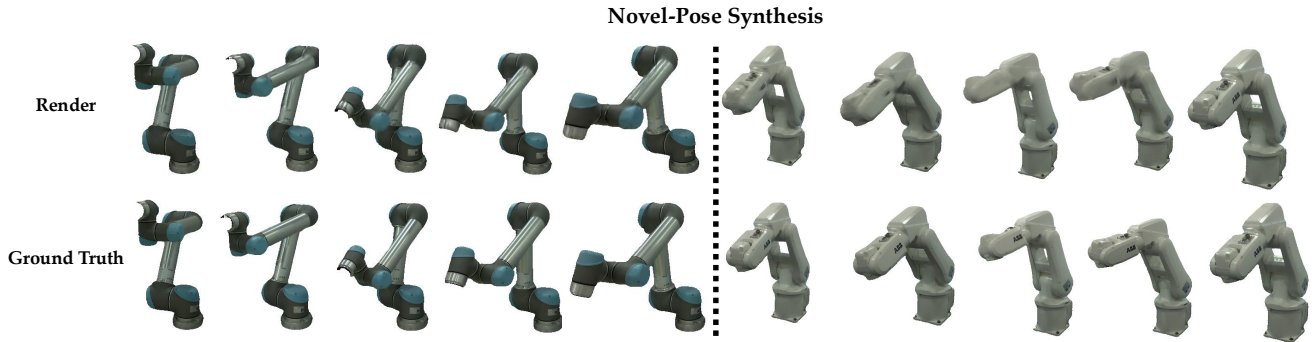


Figure 2. **Qualitative results for Novel-Pose Synthesis.** We visualize the rendered results of the robotic arms under unseen joint configurations (held-out test poses). Even in challenging poses that deviate significantly from the canonical training configurations, RoboArmGS maintains structural integrity and visual fidelity. The results demonstrate precise kinematic alignment and realistic shading changes consistent with the robot’s motion.

C. Additional Experiments Results

In this section, we provide a detailed per-scene quantitative analysis of RoboArmGS on the RoboArm4D dataset, specifically focusing on the Universal Robots UR5e and ABB IRB 120 sequences. As shown in Tab. 1, our method achieves consistently high performance across different robotic morphologies, validating the generalizability of our proposed framework.

C.1. Novel-View Synthesis

We first evaluate the static reconstruction quality on the Novel-View Synthesis task. As reported in Tab. 1, RoboArmGS achieves excellent rendering fidelity on both robotic arms. Specifically, for the Universal Robots UR5e, our method attains a PSNR of 34.92 dB and an SSIM of 0.968. Similarly, for the ABB IRB 120, we achieve a PSNR of 35.02 dB and an SSIM of 0.969. These metrics indicate that our Structured Gaussian Binding (SGB) strategy effectively leverages the underlying kinematic mesh to constrain the 3D Gaussians, allowing for precise geometry reconstruction even from monocular input. Qualitative results shown in Fig. 1 further corroborate these findings. Our method renders sharp boundaries and preserves fine-grained texture details, effectively capturing the specific visual characteristics of each robot arm without exhibiting the cloudy artifacts often seen in unconstrained Gaussian splatting.

Table 1. **Per-scene Quantitative Results on RoboArm4D.** Detailed performance of RoboArmGS on Universal Robots UR5e and ABB IRB 120. The results are reported separately for Novel-View Synthesis and Novel-Pose Synthesis tasks.

Robot	PSNR \uparrow	SSIM \uparrow	LPIPS \downarrow
<i>Novel-View Synthesis</i>			
Universal Robots UR5e	34.92	0.968	0.026
ABB IRB 120	35.02	0.969	0.038
<i>Novel-Pose Synthesis</i>			
Universal Robots UR5e	36.25	0.984	0.016
ABB IRB 120	37.36	0.982	0.018

C.2. Novel-Pose Synthesis

The Novel-Pose Synthesis task evaluates the model’s ability to generate photorealistic images under unseen joint configurations, which is critical for building actionable digital assets. Remarkably, as shown in Tab. 1, RoboArmGS achieves even higher quantitative metrics on this dynamic task, with PSNRs exceeding 36 dB and 37 dB for the UR5e and ABB arms, respectively. The LPIPS scores remain exceptionally low (< 0.02), reflecting high perceptual realism. This superior performance is attributed to our Bézier-based Motion Refiner (BMR), which successfully decouples motion artifacts from appearance learning. By compensating for the residual errors between the idealized URDF and the real-world mechanical motion, BMR ensures that the Gaussians are correctly positioned for any given input pose. Fig. 2 visualizes these results, demonstrating that the rendered arms align perfectly with the target poses while maintaining consistent lighting and occlusion handling, proving the effectiveness of our method for high-fidelity dynamic simulation.